International Journal of Solids and Structures 50 (2013) 3519–3527

Contents lists available at SciVerse ScienceDirect

International Journal of Solids and Structures

journal homepage: www.elsevier.com/locate/ijsolstr

Carbon fiber-reinforced rectangular isolators with compressible elastomer: Analytical solution for compression and bending

Paolo Angeli *, Gaetano Russo, Abramo Paschini

Department of Civil Engineering and Architecture, University of Udine, Via delle Scienze, 206, 33100 Udine, Italy

ARTICLE INFO

Article history:
Received 6 October 2012
Received in revised form 25 February 2013
Available online 4 July 2013

Keywords:
Base isolation
Fiber-reinforced elastomeric isolator
Design of isolator

ABSTRACT

The behavior of multilayer elastomeric isolators employing carbon fibers as reinforcement material rather than steel has been considered. This kind of reinforcement is used to make the isolators lighter and cheaper, since carbon fibers (or Kevlar) are much more resistant per unit weight than steel. From the mechanical point of view, the main difference is that the fiber reinforcement cannot be considered rigid in extension as it is usually done for steel plates. In this paper an analytical model to analyze the compression and bending behavior of fiber-reinforced rectangular isolators is presented. The model takes into account, for the first time, both the reinforcement extensibility and the compressibility of the elastomer. An analytical solution to predict deformations, stresses and stiffness is here determined in terms of Fourier series, both for compression and bending.

1. Introduction

Seismic isolation is a design approach to preserve structures from earthquakes loads, which is based on the considerably increase of the fundamental vibration period of structures due to isolators presence. This goal is essentially reached by utilizing devices which exhibit significant horizontal flexibility, maintaining high vertical stiffness. Steel reinforced elastomeric isolators (SREIs), usually used for seismic isolation, consist of a number of sheets of elastomeric layers alternated to thin steel plates and bonded to them. Steel plates are supposed to be rigid and consequently lateral displacements at the top and the bottom of each elastomeric layer are zero, thus increasing computed vertical stiffness. Two steel plates, much thicker than others, are positioned at the top and bottom of the whole isolator; they allow the isolator to be rigidly connected, by means of other two thick steel plates, to the foundation and to the superstructure. This kind of isolators is heavy and expensive and consequently this isolation technology is generally applied in specific cases only (emergency centers, hospitals or large-expensive buildings).

In the last years, theoretical studies have been carried out to conceive isolators lighter and possibly made by a less labor-intensive manufacturing process. Kelly (2002) and Kelly and Takhirov (2002) showed that such kind of isolators can be produced, replacing steel plates with carbon fiber sheets or Kevlar. In the following years, experimental and numerical studies (Kelly, 2002; Kelly and Takhirov, 2002; Moon et al., 2003; Russo et al., 2008; Toopchi-Nezhad et al., 2008; Mordini and Strauss, 2008; Gerhaher et al., 2009) have been carried out to verify the feasibility and reliability of such isolators.

The great advantage of this kind of isolators is that they are much lighter weighting, but fiber reinforcement exhibits extensional flexibility producing a small but significant reduction in isolators vertical stiffness, with respect to steel reinforced isolators. Therefore a good design of isolators requires a correct estimation of vertical and flexural stiffness.

Some models to evaluate vertical and flexural stiffness for carbon fiber reinforced elastomeric isolators are already present in the literature. They all assume both the elastomeric material and the fiber-reinforcement to be linearly elastic; this is allowed by the fact that displacements involved by compression and bending actions are small. Moreover, the stress state is supposed to be dominated by internal pressure (Kelly, 1997). In order to obtain analytical solutions, identical deformations are assumed for each elastomeric reinforced layer. By this way, the analysis of the overall isolator reduces on the analysis of the single fiber-reinforced elastomeric layer.

Different models can be considered, according to the different hypothesis that can be introduced on the geometry and on the mechanical properties of the materials which constitute the isolator. In particular, (i) the isolator shape can be circular, rectangular or an infinitely long strip; (ii) the reinforcement can be assumed to be rigid (typically for steel reinforcement) or extensible (fiber-reinforcement) and (iii) the elastomer can be assumed incompressible or not.

The first proposed model (Kelly, 1997) considers isolators with rigid reinforcement and compressible or incompressible rubber.

* Corresponding author.
E-mail address: paolo.angeli@uniud.it (P. Angeli).

0020-7683/$ - see front matter © 2013 Elsevier Ltd. All rights reserved.
http://dx.doi.org/10.1016/j.ijsolstr.2013.06.016

Kelly (1999) takes into account reinforcement extensibility for infinitely long isolators. For the same shape, Kelly and Takhirov (2002) considers also rubber compressibility. Tsai and Kelly (2002) study the behavior of rectangular isolators, taking into account reinforcing extensibility but neglecting rubber compressibility; they consider the reinforcement as a homogenous isotropic elastic sheet supporting shear stresses and obeying Poisson effect.

On the basis of the above mentioned approaches, in this paper an analytical model for rectangular carbon fiber-reinforced isolators, which takes into account reinforcement flexibility and rubber compressibility, is for the first time presented. In this case, the reinforcement is made by fabrics constituted with carbon fibers laid out in two orthogonal directions and simply overlapped. As it is explained in detail in the following chapter, such a kind of material does not present Poisson effect and it is not able to sustain shear stress. For this reason the reinforcement model is different from Tsai and Kelly's (2002) one.

The analytical solution for compression and bending is given in terms of Fourier series. To validate the model a Finite Element (FE) analysis has been also carried out; it showed an excellent agreement with the analytical solution.

As all above mentioned models do, the proposed one assumes a linear elastic behavior both for elastomer and the reinforcement. For this reason, the range of applicability of the obtained solution is restricted to small deformations occurring under service loading. Being the assumed behavior elastic, no damping effect can be taken into account.

Linear behavior for the materials is also assumed in the FE analysis to make the numerical model consistent with the analytical one.

2. Compression analysis

A rectangular isolator with extensible reinforcement is a system of elastomeric layers alternated with reinforcing fiber fabrics. Thickness of each elastomeric layer is t, while the ideal equivalent thickness of the fiber fabric is t_f, being the fibers volume assumed to be uniformly distributed on the whole isolator cross section. In Fig. 1 a portion of an isolator bounded by the symmetry vertical plane and constituted by three elastomeric layers, is represented.

To study the static behavior of the isolator, a single fiber-reinforced elastomeric layer extracted from the whole, as shown in Fig. 1, is considered. The single fiber-reinforced elastomeric layer is made by an elastomeric layer and by two superior and inferior fiber sheets of ideal thickness $t_f/2$ each, as represented in Fig. 2. The side length parallel to the x axis is $2b$ and to the y axis is $2h$.

2.1. Equilibrium equations in the elastomeric layer

A vertical compressive load P is supposed to be applied to the isolator layer. Each point of the elastomer exhibits the displacements u, v, and w in x, y and z coordinate directions respectively.

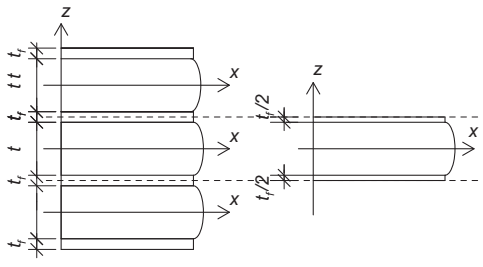

Fig. 1. Portion of the isolator and the extracted single layer.

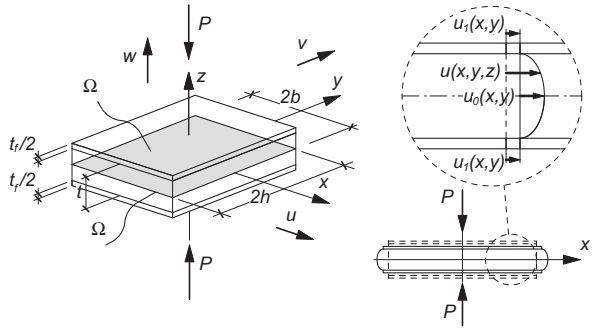

Fig. 2. Single fiber-reinforced elastomeric layer under compression and the displacements field.

By assuming fiber sheets to be perfectly bonded to the elastomeric layers, these displacements can be expressed as (Tsai and Kelly, 2002):

$$u(x,y,z) = u_0(x,y)(1 - 4z^2/t^2) + u_1(x,y) \tag{1}$$

$$v(x,y,z) = v_0(x,y)(1 - 4z^2/t^2) + v_1(x,y) \tag{2}$$

$$w(x,y,z) = w(z) \tag{3}$$

First terms on the right-hand side of Eqs. (1) and (2), represent the kinematic assumption that the displacements u and v vary quadratically along z, u_0 and v_0 being the displacements of the elastomeric layer mean plane x–y. The additional displacements u_1 and v_1, which are constant through the thickness, are the displacements evaluated at the fiber reinforcement interface. These displacements are equals to those of the fiber sheet, due to perfect bonding between elastomer and fibers. The fiber sheet displacements u_1 and v_1 are assumed to be constant along the fiber sheet thickness, due to its smallness. Eq. (3) represents the kinematic assumption that horizontal planes remain plane after the deformation. A sketch of the displacement field is shown on the right-hand side in Fig. 2.

Accordingly to the hypothesis introduced by Kelly (1997), the stress state in the elastomer is supposed to be dominated by the internal pressure p, such that the corresponding stress components are assumed to be:

$$\sigma_{xx} \approx \sigma_{yy} \approx \sigma_{zz} \approx -p \tag{4}$$

$$\tau_{xy} = \tau_{yx} \approx 0 \tag{5}$$

The equilibrium equations in x and y directions for the stresses in the elastomer are therefore reduced to (Kelly, 1997)

$$-p_{,x} + \tau_{xz,z} = 0 \tag{6}$$

$$-p_{,y} + \tau_{yz,z} = 0 \tag{7}$$

where commas imply partial differentiation with respect to the coordinate indicated after the comma.

A linear elastic behavior for the elastomer is assumed.

By taking into account the compressibility of the material, the compressibility equation can be written

$$u_{,x} + v_{,y} + w_{,z} = -\frac{p}{K} \tag{8}$$

where K is the bulk modulus of the elastomer. The right-hand side in Eq. (8) is equal to zero when the elastomer compressibility is not taken into account, as was done by Tsai and Kelly (2002).

Eqs. (1)–(8) are the governing equations of the elastic problem of rectangular isolators with extensible reinforcement and compressible elastomer. A solution of this problem is here obtained for the first time as shown in the following paragraphs.

Substituting Eqs. (1)–(3) in Eq. (8) and then integrating from $z = -t/2$ to $z = t/2$, it is obtained:

$$\frac{2}{3}(u_{0,x} + v_{0,y}) + (u_{1,x} + v_{1,y}) = \varepsilon_c - \frac{p}{K} \tag{9}$$

in which $\varepsilon_c = (w(-t/2) - w(t/2))/t$ is the axial strain measured along z in the elastomeric layer.

Eq. (9) will be the fundamental equation in terms of pressure p. To express displacements derivatives as functions of pressure, equilibrium equations will be used.

Taking into account that $\tau_{xz} = 2G\gamma_{xz} = G(u_{,z} + w_{,x})$ and $\tau_{yz} = 2G\gamma_{yz} = G(v_{,z} + w_{,y})$, with G shear modulus of the elastomer, and using Eqs. (1)–(3), the shear stress components in the elastomer are obtained:

$$\tau_{xz} = -8Gu_0\frac{z}{t^2} \tag{10}$$

$$\tau_{yz} = -8Gv_0\frac{z}{t^2} \tag{11}$$

By means of Eqs. (10) and (11), Eqs. (6) and (7) lead to:

$$p_{,x} = -8G\frac{u_0}{t^2} \tag{12}$$

$$p_{,y} = -8G\frac{v_0}{t^2} \tag{13}$$

Differentiating Eqs. (12) and (13) with respect to x and y respectively, the expressions for the axial strains in the elastomer follow:

$$u_{0,x} = -p_{,xx}\frac{t^2}{8G} \tag{14}$$

$$v_{0,y} = -p_{,yy}\frac{t^2}{8G} \tag{15}$$

2.2. Equilibrium equations in the fiber reinforcement

In Fig. 3 a sample of a real carbon fiber reinforcement fabric, made by independent very thin threads, is shown (note that carbon fiber filaments groups are only black ones). It can be easily seen that fibers laid down in orthogonal directions are actually independent. The intersections of the fibers do not determine any mechanical link, being the fibers simply overlapped. Consequently the elongation of a fiber in one direction does not determine any shortening of the fibers in the orthogonal direction, which implies that Poisson coefficient is zero. Being the carbon fiber fabric made by independent very thin threads, it obviously does not exhibit any shear stiffness. Consequently no shear stress can arise in the fibers.

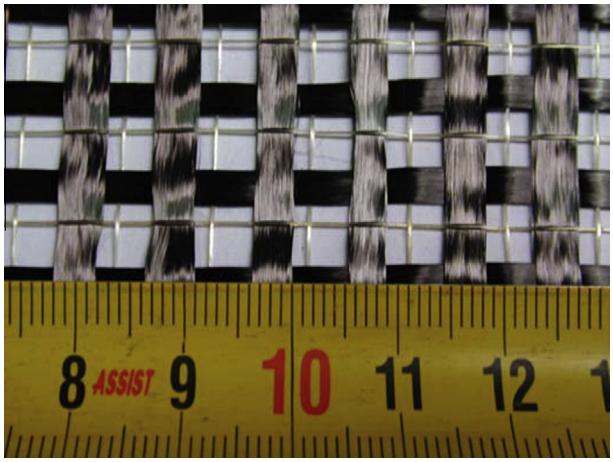

Fig. 3. A sample of a real carbon fiber fabric reinforcement.

The carbon fiber reinforcement under consideration is assumed to be constituted of continuously and uniformly distributed fibers laid in x and y directions only.

The internal forces acting on an infinitesimal area of the reinforcing sheet are therefore the forces shown in Fig. 4, where F_x and F_y represent the normal forces per unit length in x and y directions, and τ_{xz}, τ_{yz} are the shear stresses, on the surfaces of the reinforcing sheet, exerted by the elastomer.

The same fiber amount is assumed to be laid down in both directions. It follows that only half of the reinforcing thickness $t_f/2$ is laid down in one direction and half is laid down in the orthogonal one, since t_f denotes the whole ideal thickness of the fiber reinforcement fabric.

The forces F_x and F_y are therefore linearly related to the extensional strains in the respective direction only, by the following expressions:

$$u_{1,x} = \frac{2F_x}{E_f t_f} \tag{16}$$

$$v_{1,y} = \frac{2F_y}{E_f t_f} \tag{17}$$

where E_f is the elastic modulus of the fibers.

The equilibrium equations in the x and y directions are:

$$F_x + \frac{\partial F_x}{\partial x}dx + \tau_{xz}\big|^{z=-t/2}dx - F_x - \tau_{xz}\big|^{z=+t/2}dx = 0 \tag{18}$$

$$F_y + \frac{\partial F_y}{\partial y}dy + \tau_{yz}\big|^{z=-t/2}dy - F_y - \tau_{yz}\big|^{z=+t/2}dy = 0 \tag{19}$$

Taking into account Eqs. (10) and (11), Eqs. (18) and (19) provide the relationships between the displacement components in the elastomer, u_0 and v_0, and in the fibers, u_1 and v_1:

$$u_0 = -\frac{E_f t_f t}{16G}u_{1,xx} \tag{20}$$

$$v_0 = -\frac{E_f t_f t}{16G}v_{1,yy} \tag{21}$$

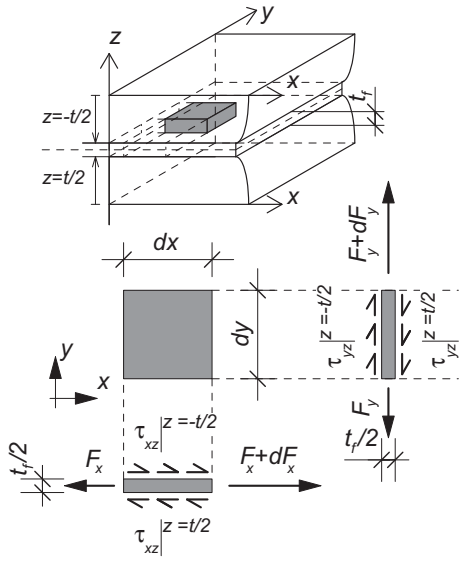

Fig. 4. Internal forces acting on an infinitesimal area of the carbon fiber reinforcing sheet.

Finally, by substituting Eqs. (20) and (21) in Eqs. (12) and (13), the following expressions are obtained:

$$p_{,x} = \frac{E_f t_f}{2t} u_{1,xx} \tag{22}$$

$$p_{,y} = \frac{E_f t_f}{2t} v_{1,yy} \tag{23}$$

Integrating Eqs. (22) and (23) with respect to x and y respectively, it is obtained:

$$p = \frac{E_f t_f}{2t} u_{1,x} + f(y) \tag{24}$$

$$p = \frac{E_f t_f}{2t} v_{1,y} + g(x) \tag{25}$$

2.3. Boundary conditions

To determine the function $f(y)$ appearing in Eq. (24), appropriate boundary conditions have to be considered: at the lateral surface of the elastomeric layer ($x = \pm b$) both the pressure p and the force F_x must be zero; taking into account Eqs. (24) and (16), this implies that $f(y) = 0$.

Analogously for $y = \pm h$ both p and F_y must be zero, implying $g(x) = 0$.

Thus from Eqs. (24) and (25), axial strains in the reinforcement as functions of the pressure p are obtained:

$$u_{1,x} = \frac{2t}{E_f t_f} p \tag{26}$$

$$v_{1,y} = \frac{2t}{E_f t_f} p \tag{27}$$

Replacing Eqs. (14) and (15) and Eqs. (26) and (27) into Eq. (9), it is obtained:

$$\nabla^2 p - (2\alpha^2 + \beta^2) p = -\frac{12G}{t^2} \varepsilon_c \tag{28}$$

where $\nabla^2 p = (p_{,xx} + p_{,yy})$ and the following constants have been introduced:

$$\alpha = \sqrt{\frac{2 \cdot 12G}{E_f t_f t}} \tag{29}$$

$$\beta = \sqrt{\frac{12G}{K \cdot t^2}} \tag{30}$$

It must be observed that, for a given elastomeric layer thickness t, α provides a measure of the elastomer shear stiffness G relative to the fiber sheet axial stiffness ($E_f t_f/2$) per unit length. So α tends to zero for axially rigid fibers.

Analogously, the parameter β provides a measure of the same shear stiffness G relative to the bulk modulus K. So β becomes zero for incompressible elastomer (i.e. when K is very large)

2.4. Solution of pressure

Eq. (28) is the partial differential equation which has to be satisfied by $p(x,y)$ within the region Ω given by the cross-section of the elastomeric layer (Fig. 2). Since no forces are applied on the lateral surface of the elastomeric layer, the following boundary conditions on the perimeter $\partial\Omega$ (Fig. 2) must hold:

$$p(\pm b, y) = 0 \quad y \in [-h, h] \tag{31}$$

$$p(x, \pm h) = 0 \quad x \in [-b, b] \tag{32}$$

To solve Eq. (28), with boundary conditions (31) and (32), Fourier series technique can be used. If the pressure p is expressed by:

$$p(x,y) = \sum_{n,m=1}^{\infty} p_{nm} \cos\left(\frac{n\pi}{2b} x\right) \cos\left(\frac{m\pi}{2h} y\right) \tag{33}$$

where the Fourier series is extended only to terms for which n and m are odd numbers, then each term of the series identically satisfies boundary conditions (31) and (32), and consequently $p(x,y)$ vanishes on the boundary.

The constant term on the right-hand side in Eq. (28) can also be expressed by means of an analogous double Fourier series:

$$-\frac{12G}{t^2} \varepsilon_c = \sum_{n,m=1}^{\infty} a_{nm} \cos\left(\frac{n\pi}{2b} x\right) \cos\left(\frac{m\pi}{2h} y\right) \tag{34}$$

where the terms a_{nm} are determined as:

$$a_{nm} = \frac{1}{bh} \int_{-b}^{b} \int_{-h}^{h} \left(-\frac{12G}{t^2} \varepsilon_c\right) \cos\left(\frac{n\pi}{2b} x\right) \cos\left(\frac{m\pi}{2h} y\right) dy dx \tag{35}$$

Substituting Eqs. (33) and (34) in Eq. (28), utilizing a_{nm} values obtained from Eq. (35) and finally equating the homologous cosine coefficients, it follows:

$$p_{nm} = \frac{\frac{192G}{mn\pi^2 t^2} \varepsilon_c}{\left(\frac{n\pi}{2b}\right)^2 + \left(\frac{m\pi}{2h}\right)^2 + (2\alpha^2 + \beta^2)} \sin\left(\frac{m\pi}{2}\right) \sin\left(\frac{n\pi}{2}\right) \tag{36}$$

Eq. (33), by means of Eq. (36), gives the final expression for $p(x,y)$:

$$p(x,y) = \sum_{n,m=1}^{\infty} \frac{192G}{mn\pi^2 t^2} \varepsilon_c \frac{\sin\left(\frac{m\pi}{2}\right) \sin\left(\frac{n\pi}{2}\right)}{\left(\frac{n\pi}{2b}\right)^2 + \left(\frac{m\pi}{2h}\right)^2 + (2\alpha^2 + \beta^2)} \times \cos\left(\frac{n\pi}{2b} x\right) \cos\left(\frac{m\pi}{2h} y\right) \tag{37}$$

2.5. Effective compression modulus

The compression stiffness of the single isolator layer E_c can be defined as:

$$E_c = \frac{P}{A\varepsilon_c} \tag{38}$$

where $A = 4bh$ is the area of the isolator. Integration of the function $p(x,y)$ given by Eq. (37) over the domain Ω, leads to the total vertical load P. Substitution of P into Eq. (38) leads to:

$$E_c = \frac{768GS^2}{\pi^4} \left(\frac{b}{h} + 1\right)^2 \sum_{n,m=1}^{\infty} \frac{\sin^2\left(\frac{n\pi}{2}\right) \sin^2\left(\frac{m\pi}{2}\right)}{n^2 m^2 \left(\left(\frac{n\pi}{2}\right)^2 + \left(\frac{m\pi}{2} \frac{b}{h}\right)^2 + 2(\alpha b)^2 + (\beta b)^2\right)} \tag{39}$$

in which S is the shape factor of the rectangular layer of the elastomer, defined as:

$$S = \frac{bh}{(b+h)t} \tag{40}$$

Normalizing the compression modulus given by Eq. (39) with respect to the quantity GS^2, the following expression can be obtained:

$$\frac{E_c}{GS^2} = \frac{768}{\pi^4} \left(\frac{b}{h} + 1\right)^2 \sum_{n,m=1}^{\infty} \frac{\sin^2\left(\frac{n\pi}{2}\right) \sin^2\left(\frac{m\pi}{2}\right)}{n^2 m^2 \left(\left(\frac{n\pi}{2}\right)^2 + \left(\frac{m\pi}{2} \frac{b}{h}\right)^2 + 2(\alpha b)^2 + (\beta b)^2\right)} \tag{41}$$

The variation of the normalized modulus E_c/GS^2 vs. αb and βb for the square isolator ($b/h = 1$) is plotted in Fig. 5.

It can be immediately noticed that, for given shape factor S and elastomeric shear modulus G, the compression modulus decreases when either αb or βb increases. The variation of the normalized

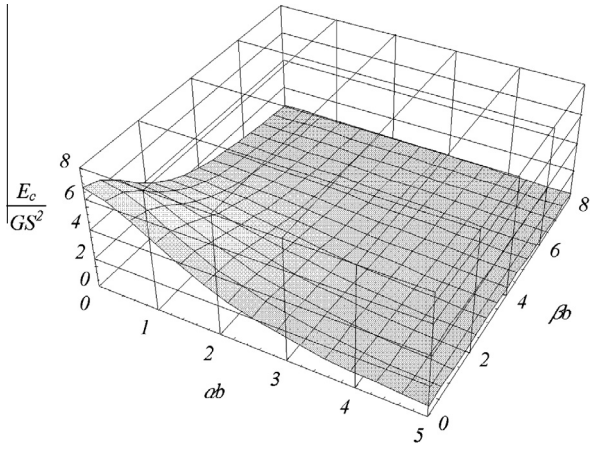

Fig. 5. Normalized effective compression modulus for a square fiber reinforced layer.

compression modulus with αb for different values of the aspect ratio b/h is plotted in Fig. 6.

These curves exhibit similar shapes to those obtained by Tsai and Kelly (2002) for isotropic homogeneous reinforcement. The upper curve in Fig. 6 coincides with the curve shown in Fig. 5 at $\beta b = 0$. In Fig. 6, it can be observed that by increasing αb, i.e. decreasing the fiber sheet axial stiffness per unit length, the normalized compression modulus rapidly decreases. Moreover it can be observed that the greatest E_c is exhibited by the square isolator ($b/h = 1$).

The variation of normalized compression modulus with βb, for different values of the aspect ratio b/h, is plotted in Fig. 7

It can be observed that by increasing βb, i.e. decreasing the bulk modulus of the elastomer, the normalized compression modulus rapidly decreases. The upper curve in Fig. 7 coincides with the curve shown in Fig. 5 at $\alpha b = 0$.

2.6. Horizontal displacements and shear stresses in the elastomer

The displacements u_0 and v_0 can be immediately calculated differentiating the expression of $p(x,y)$, Eq. (37), and substituting the result into Eqs. (12) and (13), obtaining:

$$u_0 = \frac{t^2}{8G}\sum_{n,m=1}^{\infty} p_{nm}\frac{n\pi}{2b}\sin\left(\frac{n\pi}{2b}x\right)\cos\left(\frac{m\pi}{2h}y\right) \tag{42}$$

$$v_0 = \frac{t^2}{8G}\sum_{n,m=1}^{\infty} p_{nm}\frac{m\pi}{2h}\cos\left(\frac{n\pi}{2b}x\right)\sin\left(\frac{m\pi}{2h}y\right) \tag{43}$$

Substituting Eqs. (42) and (43) into Eqs. (10) and (11) respectively, the shear stresses in the elastomer are obtained:

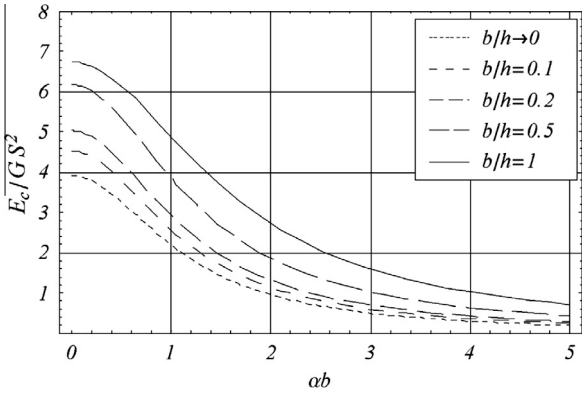

Fig. 6. Variation of normalized compression modulus with αb for an incompressible elastomer $\beta b = 0$.

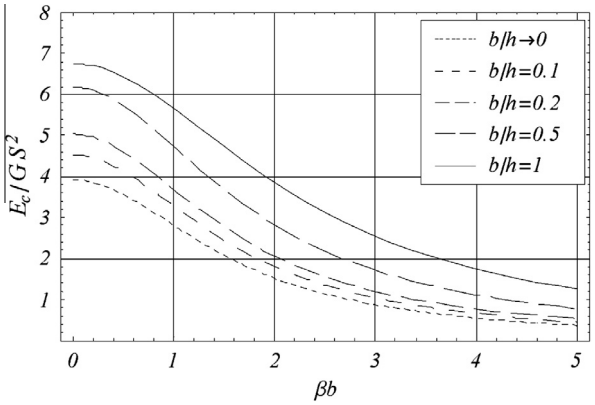

Fig. 7. Variation of normalized effective compression modulus with βb for rigid reinforcement $\alpha b = 0$.

$$\tau_{xz} = -z\frac{\pi}{2b}\sum_{n,m=1}^{\infty} p_{nm} n\sin\left(\frac{n\pi}{2b}x\right)\cos\left(\frac{m\pi}{2h}y\right) \tag{44}$$

$$\tau_{yz} = -z\frac{\pi}{2h}\sum_{n,m=1}^{\infty} p_{nm} m\cos\left(\frac{n\pi}{2b}x\right)\sin\left(\frac{m\pi}{2h}y\right) \tag{45}$$

2.7. Horizontal displacements and internal forces in the reinforcement

The displacements in the reinforcement u_1 and v_1 can be obtained by substituting the expression of $p(x,y)$, Eq. (37), into Eqs. (26) and (27) and integrating with respect to x and y respectively:

$$u_1 = \frac{4bt}{E_f t_f}\sum_{n,m=1}^{\infty}\frac{p_{nm}}{n\pi}\sin\left(\frac{n\pi}{2b}x\right)\cos\left(\frac{m\pi}{2h}y\right) + A(y) \tag{46}$$

$$v_1 = \frac{4ht}{E_f t_f}\sum_{n,m=1}^{\infty}\frac{p_{nm}}{m\pi}\cos\left(\frac{n\pi}{2b}x\right)\sin\left(\frac{m\pi}{2h}y\right) + B(x) \tag{47}$$

Because of the symmetry of the deformed isolator under the compression load P, the x-displacement of the points on the y axis must vanish ($u_1(0,y) = 0$), and consequently $A(y) = 0$. The analogous occur for the points on the x axis ($v_1(x,0) = 0$), and consequently $B(x) = 0$. It follows that:

$$u_1 = \frac{4bt}{E_f t_f}\sum_{n,m=1}^{\infty}\frac{p_{nm}}{n\pi}\sin\left(\frac{n\pi}{2b}x\right)\cos\left(\frac{m\pi}{2h}y\right) \tag{48}$$

$$v_1 = \frac{4ht}{E_f t_f}\sum_{n,m=1}^{\infty}\frac{p_{nm}}{m\pi}\cos\left(\frac{n\pi}{2b}x\right)\sin\left(\frac{m\pi}{2h}y\right) \tag{49}$$

Finally, differentiating Eqs. (48) and (49) with respect to x and y respectively, and substituting into Eqs. (16) and (17), the internal forces acting on the fiber reinforcing sheet in x and y direction follow:

$$F_x = t\sum_{n,m=1}^{\infty} p_{nm}\cos\left(\frac{n\pi}{2b}x\right)\cos\left(\frac{m\pi}{2h}y\right) \tag{50}$$

$$F_y = t\sum_{n,m=1}^{\infty} p_{nm}\cos\left(\frac{n\pi}{2b}x\right)\cos\left(\frac{m\pi}{2h}y\right) \tag{51}$$

3. Bending analysis

A layer of a rectangular isolator with extensible reinforcement subjected to a pure bending moment M about the y-axis, is shown in Fig. 8. Due to the bending moment M, top and bottom surfaces

rotate about the y-axis. Fiber reinforcement sheets are assumed to remain plane and the angle between two consecutive reinforcing sheets is denoted by θ

3.1. Governing equations

The kinematic assumptions for the displacements in x and y direction, are the same used in the compression analysis (Eqs. (1) and (2)), while the displacements of the elastomer in the z direction is given by (Kelly, 1999):

$$w(x,y,z) = \theta z \frac{x}{t} \tag{52}$$

which evidences that horizontal planes rotate rigidly about y-axis, but remain plane after deformation.

In the following, the procedure goes through the same analytical steps of the compression problem.

Substituting Eqs. (1), (2), and (52) into the compressibility equation, Eq. (8), and then integrating from $z = -t/2$ to $z = t/2$ lead to:

$$(u_{0,x} + v_{0,y}) + \frac{3}{2}(u_{1,x} + v_{1,y}) = -\frac{3}{2}\frac{\theta x}{t} - \frac{3}{2}\frac{p}{K} \tag{53}$$

Eq. (8), by using Eqs. (1), (2), and (52), provides the shear stress τ_{xz} in the elastomer:

$$\tau_{xz} = -8Gu_0\frac{z}{t^2} + G\frac{\theta}{t}z \tag{54}$$

while τ_{yz} is still provided by Eq. (11).

Substitution of Eq. (54) into Eq. (6), leads to:

$$p_{,x} = -8G\frac{u_0}{t^2} + \frac{G\theta}{t} \tag{55}$$

while $p_{,y}$ is still provided by Eq. (13)

Derivation of Eq. (55) with respect to x, leads again to Eq. (14).

Although expression (54) for τ_{xz} exhibit an extra term with respect to that given by Eq. (10), relevant to the compression case, Eqs. (14) and (15) and Eqs. (22)–(27) can be obtained unaltered in the bending case.

Replacing Eqs. (14) and (15) and Eqs. (26) and (27) into Eq. (53), it is obtained:

$$\nabla^2 p - (2\alpha^2 + \beta^2)p = \frac{12G}{t^2}\frac{\theta x}{t} \tag{56}$$

As it can be easily seen, the only difference with respect to Eq. (28) relies on the axial strain appearing on the right-hand side which, instead to be constant, varies linearly along x-axis in the bending case.

Eq. (56) is the partial differential equation which has to be satisfied by $p(x,y)$ within region Ω (Fig. 2). The boundary conditions on the perimeter $\partial\Omega$ (Fig. 2) of the elastomeric layer are provided again by Eqs. (31) and (32).

3.2. Solution of pressure

To solve the problem given by Eqs. (56), (31), and (32), Fourier series technique can be used. Consequently the pressure p is expanded in the following way:

$$p(x,y) = \sum_{n,m=1}^{\infty} p_{nm} \sin\left(\frac{n\pi}{b}x\right)\cos\left(\frac{m\pi}{2h}y\right) \tag{57}$$

where, in this case, $n = 1,2,3,4\ldots$ and $m = 1,3,5\ldots$, to identically satisfy boundary and symmetry conditions. In fact p must be an odd function with respect to y direction and an even function with respect to x direction.

Analogously the known term in the right-hand side of Eq. (56) can be expanded as:

$$\frac{12G}{t^2}\frac{\vartheta x}{t} = \sum_{n,m=1}^{\infty} a_{nm} \sin\left(\frac{n\pi}{b}x\right)\cos\left(\frac{m\pi}{2h}y\right) \tag{58}$$

with $n = 1,2,3,4\ldots$ and $m = 1,3,5\ldots$ The terms a_{nm} are determined by calculating the following integrals:

$$a_{nm} = \frac{1}{bh}\int_{-b}^{b}\int_{-h}^{h}\left(\frac{12G}{t^2}\frac{\theta x}{t}\right)\sin\left(\frac{n\pi}{b}x\right)\cos\left(\frac{m\pi}{2h}y\right)dydx \tag{59}$$

Substituting a_{nm} expressions obtained from Eq. (59) into Eq. (58) and utilizing also Eqs. (57) and (56) provides the series expressions from which, equating the homologous sine and cosine coefficients, the p_{nm} coefficients are derived:

$$p_{nm} = \frac{\frac{96Gb}{mn^2\pi^3t^2}\frac{\theta}{t}\sin\left(\frac{m\pi}{2}\right)(n\pi\cos(n\pi) - \sin(n\pi))}{\left(\frac{n\pi}{b}\right)^2 + \left(\frac{m\pi}{2h}\right)^2 + (2\alpha^2 + \beta^2)} \tag{60}$$

By means of Eq. (60), Eq. (57) provides the final expression for the pressure $p(x,y)$ in the elastomer:

$$p(x,y) = \sum_{n,m=1}^{\infty} \frac{\frac{96Gb}{mn^2\pi^3t^2}\frac{\theta}{t}\sin\left(\frac{m\pi}{2}\right)(n\pi\cos(n\pi) - \sin(n\pi))}{\left(\frac{n\pi}{b}\right)^2 + \left(\frac{m\pi}{2h}\right)^2 + (2\alpha^2 + \beta^2)} \times \sin\left(\frac{n\pi}{b}x\right)\cos\left(\frac{m\pi}{2h}y\right) \tag{61}$$

3.3. Effective bending modulus

The effective bending modulus of the single isolator layer of the elastomer E_b can be defined as:

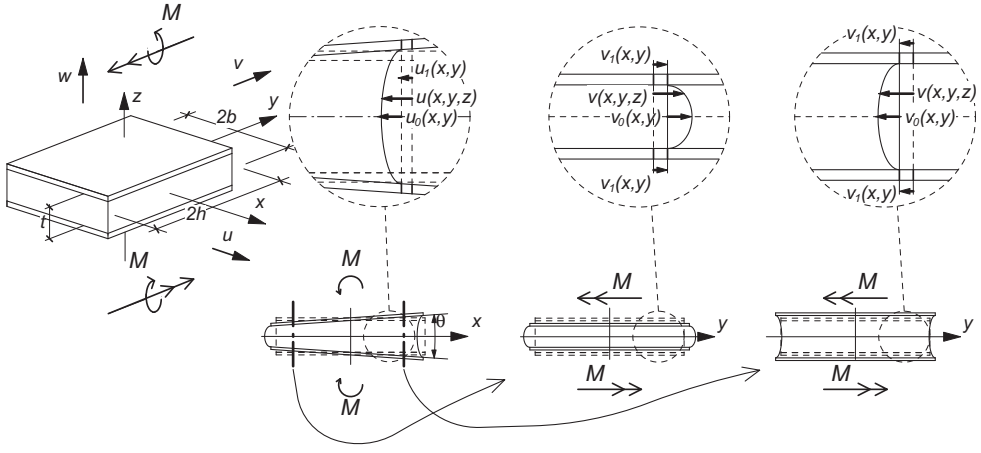

Fig. 8. Rectangular layer of reinforced elastomer under pure bending.

$$E_b = \frac{M}{I_y \frac{\theta}{t}} \tag{62}$$

where $I_y = 4/3b^3h$ is the moment of inertia about the y axis of the rectangular area, and M is the bending moment, which can be expressed as:

$$M = -\int_{-b}^{b}\int_{-h}^{h} pxdydx \tag{63}$$

By substituting Eq. (61) into Eq. (63), the M expression is obtained, that leads Eq. (62) to give:

$$E_b = \frac{576G}{t^2\pi^6}\sum_{n,m=1}^{\infty}\frac{1}{m^2n^4}\frac{\sin\left(\frac{m\pi}{2}\right)^2}{\left(\frac{n\pi}{b}\right)^2+\left(\frac{m\pi}{2h}\right)^2+(2\alpha^2+\beta^2)}(\sin(n\pi) - n\pi\cos(n\pi))^2 \tag{64}$$

The variation of the normalized effective bending modulus (E_b/GS^2) vs. αb and βb for the square isolator ($b/h = 1$) is plotted in Fig. 9. It can be noticed that, for given shape factor S and elastomeric shear modulus G, the bending modulus decreases when either αb or βb increases.

The variation of normalized effective bending modulus with αb for different values of the aspect ratio b/h is plotted in Fig. 10.

All the considerations emphasized in the paragraph 2.5 can be repeated here for the bending case.

The variation of normalized effective bending modulus (E_b/GS^2) with βb, for different values of the aspect ratio b/h is plotted in Fig. 11.

The comparison of Figs. 9–11 with Figs. 5–7 respectively, shows that the effective bending modulus varies analogously to the effective compression modulus. It follows that for the effective bending modulus can be repeated the same considerations provided for the compression case (see paragraph 2.5).

3.4. Horizontal displacements and shear stresses in the elastomer

The displacements u_0 and v_0 can be obtained from Eqs. (55) and (13) by utilizing Eq. (61):

$$u_0 = -\frac{t^2}{8G}\sum_{n,m=1}^{\infty} p_{nm}\frac{n\pi}{b}\cos\left(\frac{n\pi}{b}x\right)\cos\left(\frac{m\pi}{2h}y\right)+\frac{\theta t}{8} \tag{65}$$

$$v_0 = \frac{t^2}{8G}\sum_{n,m=1}^{\infty} p_{nm}\frac{m\pi}{2h}\sin\left(\frac{n\pi}{b}x\right)\sin\left(\frac{m\pi}{2h}y\right) \tag{66}$$

Shear stresses τ_{xz} and τ_{yz} are given by Eq. (65) with Eq. (54), and by Eq. (66) with Eq. (11), respectively:

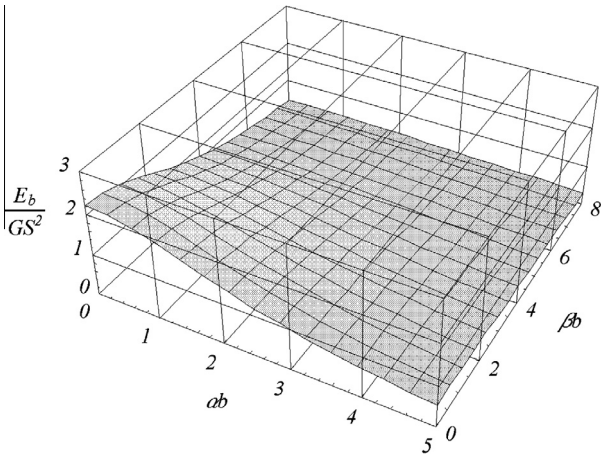

Fig. 9. Variation of normalized effective bending modulus with αb and βb.

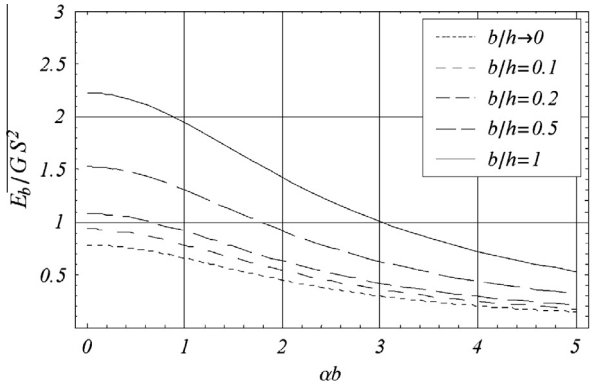

Fig. 10. Variation of normalized mean bending modulus with αb, for an incompressible elastomer $\beta b = 0$.

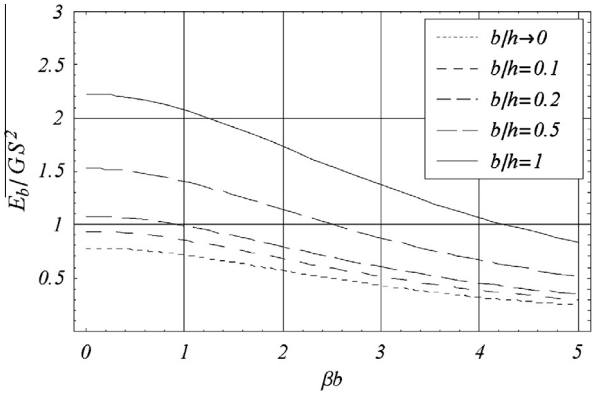

Fig. 11. Variation of normalized effective bending modulus with βb for a rigid reinforcement $\alpha b = 0$.

$$\tau_{xz} = z\frac{\pi}{b}\sum_{n,m=1}^{\infty} np_{nm}\cos\left(\frac{n\pi}{b}x\right)\cos\left(\frac{m\pi}{2h}y\right) \tag{67}$$

$$\tau_{yz} = -\frac{z\pi}{2h}\sum_{n,m=1}^{\infty} mp_{nm}\sin\left(\frac{n\pi}{b}x\right)\sin\left(\frac{m\pi}{2h}y\right) \tag{68}$$

Substituting Eq. (61) into Eq. (26) and integrating along x direction, leads to the expression u_1 for the fiber x-displacement:

$$u_1 = -\frac{2t}{E_f t_f}\sum_{n,m=1}^{\infty} p_{nm}\frac{b}{n\pi}\cos\left(\frac{n\pi}{b}x\right)\cos\left(\frac{m\pi}{2h}y\right)+A(y) \tag{69}$$

The fiber displacement in the x direction, u_1, has been determined to within a function, $A(y)$. This indeterminacy has no effect on strains and stresses, because these are determined deriving the function u_1 with respect to x.

Substituting Eq. (61) into Eq. (27) and integrating with respect to the y direction leads to:

$$v_1 = \frac{4ht}{E_f t_f}\sum_{n,m=1}^{\infty}\frac{p_{nm}}{m\pi}\sin\left(\frac{n\pi}{b}x\right)\sin\left(\frac{m\pi}{2h}y\right)+B(x) \tag{70}$$

Applying symmetry condition, $v_1(x,0) = 0$, it is obtained $B(x) = 0$. Therefore:

$$v_1 = \frac{4ht}{E_f t_f}\sum_{n,m=1}^{\infty}\frac{p_{nm}}{m\pi}\sin\left(\frac{n\pi}{b}x\right)\sin\left(\frac{m\pi}{2h}y\right) \tag{71}$$

Differentiating Eqs. (69) and (71) with respect to x and y respectively, and substituting in Eqs. (16) and (17) the normal forces per unit length acting on the fiber reinforcing sheet in x or y direction, are obtained:

$$F_x = t\sum_{n,m=1}^{\infty} p_{nm}\sin\left(\frac{n\pi}{b}x\right)\cos\left(\frac{m\pi}{2h}y\right) \tag{72}$$

$$F_y = t\sum_{n,m=1}^{\infty} p_{nm}\sin\left(\frac{n\pi}{b}x\right)\cos\left(\frac{m\pi}{2h}y\right) \tag{73}$$

4. Comparison of analytical solution and Finite Element analysis

Static behavior of some samples of rectangular fiber-reinforced isolator layers have been numerically analyzed. The geometry of the isolator and the mechanical properties of the elastomer are assumed to coincide with those used by Kelly and Takhirov (2002) in their experiments. The layer side lengths parallel to the x and y axis are $2b = 0.183$ m and $2h = 0.377$ m respectively ($b/h = 0.48$). The elastomeric layer thickness is $t = 0.003$ m. The elastomer shear and the bulk modulus are assumed to be $G = 0.69$ MPa and $K = 2000$ MPa respectively. The reinforcement thickness is $t_f/2 = 0.00027$ m in both x and y directions. More than one value for E_f has been considered in the numerical analysis; the first one, $E_f = 14{,}000$ MPa, actually unrealistic for carbon fiber reinforcement, is the value estimated by Kelly and Takhirov (2002) from their experimental compression tests on elastomeric isolation bearings. For the above mentioned values it is obtained $\alpha b = 2.47$ and $\beta b = 1.96$. The numerical analysis has been carried out by means of the ALGOR FEMPRO 13.28-WIN 13-JAN-2003 version. The elastomeric layer has been modeled through 3D elements ("brick" elements), whereas the reinforcement has been modeled with 1D elements ("truss" elements). A "Static Stress with Linear Material Model Analysis" type was carried out.

4.1. Compression

Normalized effective compression modulus E_c and pressure p values obtained by means of this numerical analysis have been compared with those analytically obtained from. Eqs. (41) and (37) reported in the previous paragraphs.

The normalized effective compression modulus (41) is plotted vs. αb in Fig. 12. Two curves have been obtained from Eq. (41): the upper one relates to an incompressible elastomer, i.e. $K \to (\beta b = 0)$, which cannot be numerically analyzed because of numerical instabilities, and the lower one relates to an elastomer with $K = 2000$ Mpa ($\beta b = 1.96$).

For the previously mentioned case ($\alpha b = 2.47$ and $\beta b = 1.96$) numerical analysis leads to a normalized compression modulus E_c/GS^2 value equal to 1.12 (point A in Fig. 12). The value obtained by means of the proposed Eq. (41) results 1.10. The difference between these values is 2%.

Since the above used E_f value is very low for carbon fiber reinforcement, as stated by Kelly himself, fiber reinforcement stiffness ($E_f t_f/2$) 4, 8 and 16 times greater than that relating to the first case, are considered. The normalized effective compression modulus values obtained by means of numerical analyses are represented in Fig. 12 by the points B, C and D respectively. It can be observed that the analytical curve plot is very close to the four numerically obtained points, thus evidencing the validity of the proposed analytical model.

For the case $\alpha b = 2.47$ and $\beta b = 1.96$ point A in Fig. 12, the normalized pressure distributions $p/(E_c \cdot \Delta/t)$ along x direction for $y = 0$ and along y for $x = 0$, are shown in Figs. 13 and 14 respectively. Continuous lines represent distribution derived analytically from Eq. (37), whereas isolated points show numerical results obtained from FE analysis.

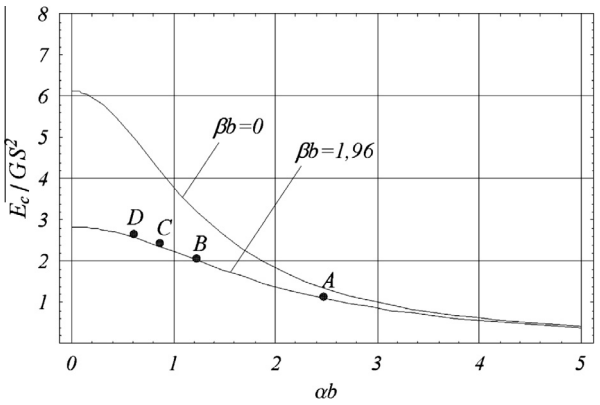

Fig. 12. Effective compression modulus: analytical and numerical test results.

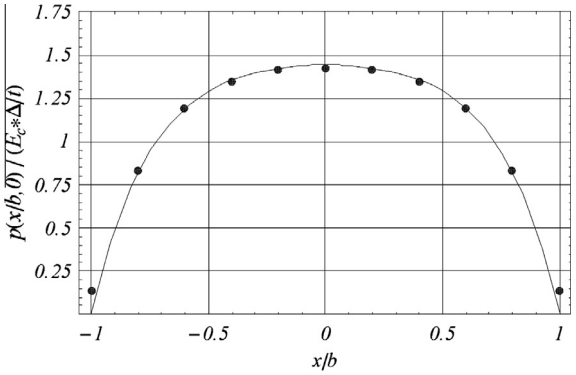

Fig. 13. Distribution of normalized pressure p with x, at $y = 0$.

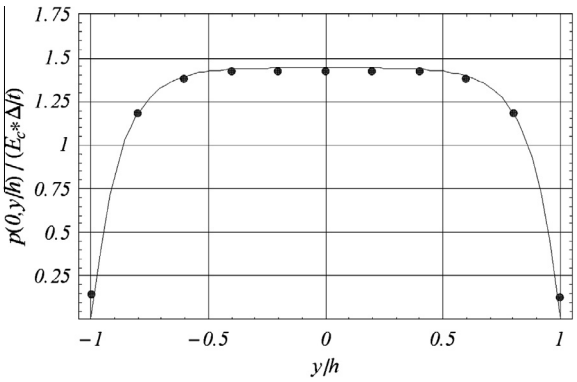

Fig. 14. Distribution of normalized pressure p with y, at $x = 0$.

The curves obtained by means of the proposed model are very close to numerical values, thus confirming the validity of the proposed model.

4.2. Bending

The effective normalized bending modulus E_b/GS^2 for the values $\alpha b = 2.47$ and $\beta b = 1.96$ provided by the proposed Eq. (64) results 0.65, whereas using the numerical analysis it results 0.68. Latter value is reported by point A in Fig. 15. The difference between the values is 5%.

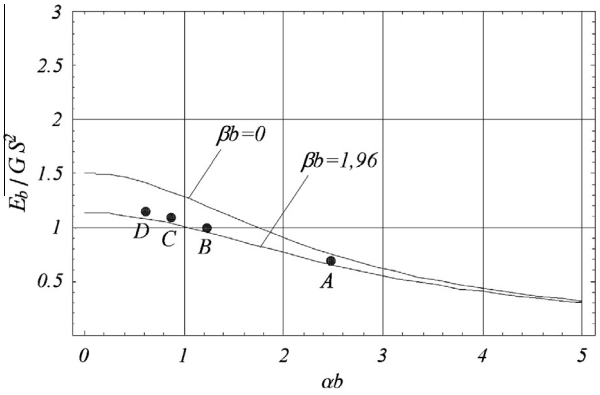

Fig. 15. Effective bending modulus: analytical and numerical test results.

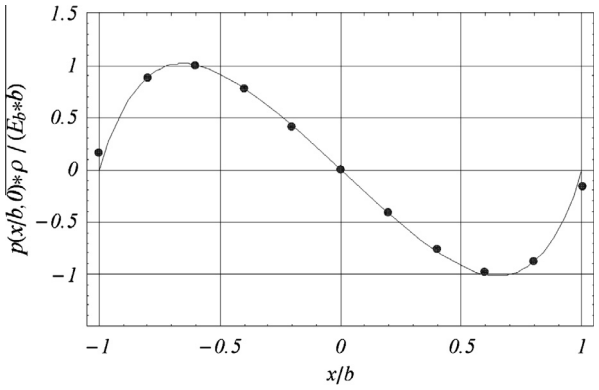

Fig. 16. Distribution of normalized pressure p with x, for $y = 0$.

Points B, C and D in Fig. 15 show numerically normalized effective bending moduli obtained considering the reinforcement to be 4, 8 and 16 times stiffer.

For the case $\alpha b = 2.47$ and $\beta b = 1.96$ (point A in Fig. 15), the normalized pressure distribution $p \cdot \rho E_b \cdot b$) along x direction, is shown in Fig. 16 for $y = 0$. Continuous line represents analytical distribution derived from Eq. (61), whereas isolated points show distribution of pressure p obtained from FE analysis.

Also in the bending case, numerical and analytical results are very close, thus confirming the validity of the proposed model.

5. Conclusions

An analytical analysis on the behavior of elastomeric rectangular isolators, with carbon fiber reinforcement and subjected to compression and bending loads, has been carried out. In particular the behavior of a single elastomeric layer bonded to fabrics constituted with carbon fibers laid out in two orthogonal directions has been considered. The elastomer has been assumed to be linear elastic and compressible. The fibers have been supposed flexible in extension.

Two new solutions in form of Fourier series expansion have been found, for compression and bending respectively. The results derived in terms of stresses, displacements and stiffness have been compared with FE numerical analysis results. Excellent agreement between analytical and FE approaches results for stresses, displacements and stiffness moduli. In particular the maximum errors have been obtained for the analytical evaluation of the compression and bending effective moduli, and it is about 2% and 5% respectively.

For design purposes, the most valuable results are formulas for predicting the compression and bending effective moduli. Regarding to these formulas, it can be concluded that:

- compression and bending stiffness moduli can be expressed as Fourier series expansions;
- the series are rapidly convergent, so that only few terms may be considered in the calculus.

Both previous conclusions makes the calculus very easier compared with FE one, the latter requiring a new numerical model when a single geometric parameter is changed.

References

Gerhaher, U., Strauss, A., Bergmeister, K., 2009. Effectiveness of a seismic isolation system for buildings using fiber reinforced elastomeric bearings. Bautechnik 86 (1), 14–21.

Kelly, J.M., 1997. Earthquake-Resistant Design with Rubber, second ed. Springer-Verlag, London.

Kelly, J.M., 1999. Analysis of fiber-reinforced elastomeric isolators. Journal of Seismology and Earthquake Engineering 2, 19–34.

Kelly, J.M., 2002. Seismic isolation systems for developing countries. Earthquake Spectra 18 (3), 385–406.

Kelly, J.M., Takhirov, S.M., 2002. Analytical and experimental study of fiber-reinforced strip isolators. PEER Rep. 2002/11, Pacific Earthquake Engineering Research Center, Univ. of California, Berkeley, California.

Mordini, A., Strauss, A., 2008. An innovative earthquake isolation system using fibre reinforced rubber bearings. Engineering Structures 30 (10), 2739–2751.

Moon, B.Y., Kang, G.J., Kang, B.S., Kim, G.S., Kelly, J.M., 2003. Mechanical properties of seismic isolation system with fiber-reinforced bearing of strip type. International Applied Mechanics 39 (10), 1231–1239.

Russo, G., Pauletta, M., Cortesia, A., Dal Bianco, A., 2008. Experimental behavior of carbon fiber reinforced isolators. In: Proceedings of the 2008 Seismic Engineering International Conference commemorating the 2008 Messina and Reggio Calabria Earthquake, 8–11 July 2008, Reggio Calabria and Messina, Italy.

Toopchi-Nezhad, H., Tait, M.J., Drysdale, R.G., 2008. Testing and modeling of square carbon fiber-reinforced elastomeric seismic isolators. Structural Control and Health Monitoring 15 (6), 876–900.

Tsai, H.C., Kelly, J.M., 2002. Stiffness analysis of fiber-reinforced rectangular seismic isolators. Journal of Engineering Mechanics 128 (4), 462–470.